This paper appears in IEEE ASME Transactions on Mechatronics 2014
http://dx.doi.org/10.1109/TMECH.2013.2291966

Design Considerations for Magnetorheological Brakes

Carlos Rossa, Adrien Jaegy, José Lozada, and Alain Micaelli

***Abstract*— Design considerations for magnetorheological (MR) brakes are discussed for different geometries. A complete modelling in terms of torque density, efficiency, bandwidth and controllability is presented. The model assigns a desired magnetic flux density over the fluid surface. The magnetic circuit dimensions and the necessary power can be calculated in consequence. The analysis focuses on a single disc and on a single drum brake and highlights the interdependence of the measures of performance as a function of the dimensions. The proposed models have been validated using finite element analysis, the results demonstrate that both brakes are equivalent in terms of torque density but drum brakes are more reactive and require less power. The analysis has subsequently been extended to multiple-layered brakes with several fluid gaps in parallel. The performance are globally improved by increasing the number of gaps. Finally, the paper considers the influence of the MR fluid characteristics an the housing material.**

1. Introduction

A magnetorheological (MR) fluid is an active material composed of a suspension of soft ferromagnetic micron-sized particles (typically 1 to 10 microns) dispersed in a carrying liquid (mineral oils, synthetic oils or water) [1][2]. Their volume concentration in the fluid may range typically between 20% and 40% [3]. The rheological properties of this material can be strongly and reversibly modified by the action of an external magnetic field [4]. It induces the magnetization of the particles which form chain-like structures or aggregates aligned roughly parallel to the magnetic field [5]. As a consequence, MR fluids posses the ability to achieve a wide range of apparent viscosity [6]. This phenomenon is macroscopically manifested when the fluid is sheared by the development of a yield stress which increases with the magnitude of the applied field in a fraction of a millisecond [7][8].

In the absence of a field, an MR fluid can be considered as a Newtonian fluid. The Herschel-Bulkley [9] and Bingham models [10] are the commonly used plastic models employed to describe the non-linear behaviour of MR fluids as a function of the magnetic field. The Herschel-Bulkley model allows a non-linear post-yield behaviour while the Bingham model assumes a linear behaviour. The constitutive formulation of the Bingham model is presented in Equation (1), where $\tau(\dot{\gamma}, H)$ is shear stress, and $\dot{\gamma}$ is shear strain rate. The fluid yield stress $\tau_y(H)$ is a function of the external magnetic field H.

MR-based actuators can be classified as having either a valve mode, a direct shear mode or a squeeze film compression mode as presented in Fig.1 [11][12]. The fluid is confined between two magnetic poles. On the shear mode, a relative displacement of the poles is induced by the action of an external force. The chain-like structures create a resistive force against the motion. On the valve mode the poles are immobilized and the magnetic field is adjusted to control the pressure drop between the input and output and therefore, the fluid flow resistance. On the compression mode, a force is imposed perpendicularly to the poles and the fluid is compressed.

The authors are with the French Atomic Energy Commission; CEA, LIST, Sensorial and Ambient Interfaces Laboratory, 91191 Gif-sur-Yvette, France. rossa@ualberta.ca; joselozada@uti.edu.ec; alain.micaelli@cea.fr.

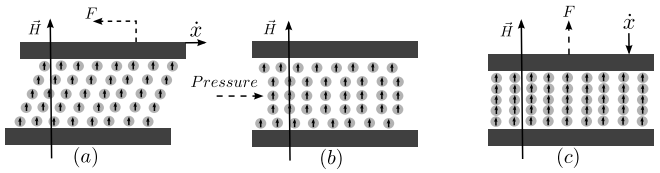

Fig. 1. Typical utilization modes of MR fluids: shear mode (a), valve mode (b) and compression mode (c), with F the braking force and $\dot{x}$ the velocity of the poles.

$$\tau(\dot{\gamma}, H) = |\tau_y(H)| + \eta|\dot{\gamma}| \tag{1}$$

In virtue of its high controllability, fast response time, very low power requirements and high torque per volume ratio, MR actuators hold great potential in many applications requiring controllable electromechanical interfaces such as clutches [13][14], brakes [15][16], valves [17][18], dampers for vibration control [19][20], robotics applications [21][22][23], and haptic devices [24][25][26].

Usually, rotary brakes are based on the shear mode and take the form of disc or drum housings as shown in Fig. 2 [27][28]. In disc brakes (Fig. 2(a)) the fluid is contained in a circular volume perpendicular to the rotation axis and the magnetic flux is applied orthogonally against the fluid shear. In drum brakes (Fig. 2(b)), the fluid is in a cylindrical gap around the rotation axis. In both cases, the tangential resistive force is calculated by integrating the field dependent yield stress $\tau(H)$ over the active contact surface S. The term "active surface" defines all fluid surface employed to create a controllable torque T. Taking into account the radius R between the fluid surface and the rotation axis, the torque is given by:

$$T = \int\int R\tau(H)dS \tag{2}$$

Disc-type brakes are used widely in a large range of domains [23]. An example is the system proposed by McDaniel [29] composed of a clutch and a brake linked in series. Li and Du [30] present a high-efficiency single disc brake and conclude that the uncontrollable viscous torque increases strongly with the rotary velocity. Li et al. [31] use a disc brake to develop a 2-DOF joystick for virtual reality applications. Karakoc et al. [32] present an automotive brake which provides 23Nm at 1.8A. Assadsangabi et al. [33] discuss the optimization of disc-type brakes in terms of maximum torque.

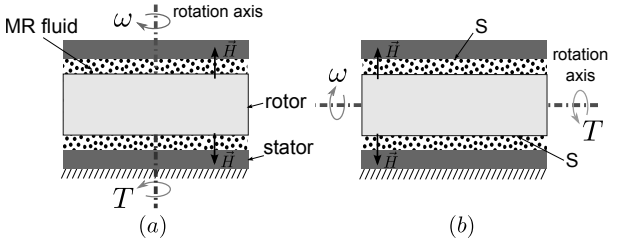

Fig. 2. Schematic view of drum and disc brake configurations. The fluid is placed between two discs for the disc type (a) and two concentric cylinders in the drum brake (b). The braking torque T against the velocity ω is generated over the active surface S, and controlled by a magnetic field H.

According to Kikuchi and Kobayashi [27], drum-brakes can effectively transduce the MR effect in braking torque with lower inertia compared to disc brakes. Huang et al. [34] develop a theoretical design method of a cylindrical brake using Bingham model and determine the parameters of the the fluid gap when the mechanical power, velocity, and dynamic range are specified. Shiao and Chang [35] optimize a drum brake by increasing the active chaining area using a multiple-pole configuration. Avraam et al. [36] develop a rehabilitation device with optimized volume and mass. Rosenfeld and Wereley [37] demonstrate the optimization of a cylindrical valve with constrained volume and conclude that small changes in the fluid gap drastically affects its performance. Nguyen et al. [38][39] describe a hybrid brake combining a disc and cylinder based in a T-shaped and U-shaped ferromagnetic core.

Multiple-layered brakes with several discs or cylinders in parallel, are an efficient way to improve the torque density. Multiple-layered disc brake, for example, is commonly employed in the design of electro-rheological (ER) actuators [40][41]. Several works have reported its implementation in high torque applications using MR fluids too [42][43][14]. Nguyen and Choi [44] use a tooth-shaped disc-type able to display 1025Nm for an automotive brake with limited dimensions and optimized weight. Shafer and Kermani [45] and Kikuchi et al. [46] chose a multiple-disc high torque clutch for human-robot interaction. Guo and Liao [47] present the optimization of multiple-disc clutch/brake comparing models with different configurations of inner coils.

Nikitczuk et al. [40] report on the design of a multi-layered drum brake using ER fluid for rehabilitation devices. Periquet and Lozada [16] chose a multiple cylinder configuration for a 1.7Nm miniature MR brake and achieved high performance in terms of torque density and power consumption.

1.1 Selection of a Brake Design

Four main configurations comprising single drum and disc brakes and their extension using multi-layered design can be identified. Using finite element analysis, Nguyen and Choi [39] compare single brakes in terms of maximum torque and volume ratio. Their results suggest that disc brakes produce more torque than cylindrical brakes for small values of radius/length ratio. Avraam [48] presents an analysis of single and multiple disc and single cylinder brakes in term of torque density, power, controllable and viscous torque expressed as a function of the fluid yield stress. In this paper the analysis is extended to multiple cylinder brakes taking also into consideration the reactivity of each brake type. The figures of merit are expressed as a function of a desired induction of the fluid. Thus, the ferromagnetic path volume and the coil characteristic are considered. This analysis allows for the identification of design tradeoffs. Knowing the evolution of the performance as a function of the geometry, different brake designs can be compared according to different criteria.

Section 2 defines the measure of performance of MR brakes. In Section 3, single drum and disc brakes are treated. All parameters are analytically calculated as a function of the geometry assuming linear relationships. The results show that for a given volume both brakes display an equivalent torque density but drum brakes can assume a larger range of external forms and are more reactive. However, drum brakes need higher power supply. In Section 4, the analysis is extended to multiple-layered brakes. The results demonstrate that the measures of performance are globally improved by increasing the number of fluid gaps. Finally, Section 5 considers the influence of the fluid and of the housing material characteristics.

2. Evaluation Criteria for MR Brakes

In the design of an MR brake, all parameters are interconnected and may have opposite influence on the performance. According to Fauteux et al. [14], a versatile actuator possesses high torque density, sufficient bandwidth and very low output impedance. Karakoc et al. [32] and Park et al. [49] focus on the optimization of the torque-to-weight ratio. Gudmundsson et al. [43] develop a multi-objective optimization method for a prosthetic knee brake in terms of controllable braking torque, off-state rotary stiffness and weight. Zhang et al. [50] focus on the finite element analysis of the magnetic circuit of a damper. For Yang et al. [51], the relation volume fraction to yield stress, response time of the coils and electric power losses should directly be used in the integral design too. As measure of performance, this paper considers the torque density, efficiency, controllability and bandwidth.

2.1 Torque density

The first evaluation criterion is the torque density. It is obtained by dividing the maximum torque T_{max} by the total volume V_t. The maximal torque corresponds to the achieved torque when a specified magnetic flux density B_d is reached over the fluid surface. The torque density ρ is computed as $\rho = T_{max}/V_t$.

2.2 Efficiency

The efficiency is defined as the ratio between the torque T_{max} and the power supply P_{max}. The proposed model considers that there is no limitation of the supplied power or input current. A linear relationship can be obtainded by dimensioning the magnetic paths in order to avoid magnetic circuit saturation [52]. Ideally, the magnetic induction of the fluid and of the ferromagnetic circuit should reach their saturation at the same electric power corresponding to P_{max} [53]. The efficiency E is then defined as $E = T_{max}/P_{max}$.

2.3 Controllability

The controllability is defined as the ratio controllable torque T_{max} to viscous friction coefficient. According to the Bingham model (Eq. 1), MR fluids present a viscous stress proportional to the shear strain rate. It represents an uncontrollable viscous torque T_f which depends on the rotational velocity ω. To overcome this dependence, we consider the ratio viscous torque to velocity $T_v = T_f/\omega$. The controllability K, represents the relation between the controllable and uncontrollable torque and is computed as $K = T_{max}/T_v$.

2.4 Reactivity

The bandwidth is limited by the time constant of the electromagnetic circuit δt_c and the response time of the fluid. An MR fluid needs less than 1ms shifting from fluid to semi-solid state [54]. Thus, the response time of the fluid is negligible compared to the electromagnetic response time which depends on the coil design and the magnetic reluctance perceived by the coil [55]. The coil is concentric to the rotation axis and is dimensioned to provide the power supply P_{max}. The ratio torque/time constant characterizes the reactivity of the brake δt_c in terms of Nm/s, for a step-type excitation, and is computed as $\delta t = T_{max}/\delta t_c$.

Section 3 presents the modelling for the two basic brake configurations with regards to these evaluation criteria.

3. Basic Rotary Brake Geometries

The indexes "d" and "c" refer to disc and to cylindrical brakes respectively. In the following models, a desired magnetic field over the active fluid surface is assigned. Subsequently, the magnetic circuit is optimally designed to provide the required field regardless the dimensions.

3.1 Disc-Shaped Brakes

A disc-shaped brake is illustrated in Fig. 3. The magnetic flux $\Phi(t)$ generated by a coil with N turns and by a current $i(t)$ is given by $\Phi(t) = Ni(t)/\mathscr{R}$. Where $\mathscr{R}$ is the magnetic reluctance observed by the coil. The relative permeability of commercial MR fluids may range from 4 to 6.5 [56][57]. On average, the permeability of the ferromagnetic path made in iron is 2000 times superior. Therefore, for usual brake dimensions, its reluctance can be neglected compared to the reluctance of the fluid. If we note g, μ_{mr}, r, and R the fluid gap depth, the absolute permeability of the fluid, the inner and external radius of the fluid gap, the active surface is $S = \pi(R^2 - q^2)$ and the reluctance can be computed as [32]:

$$\mathscr{R}_d = \sum_{k=1}^{n} \frac{g}{\mu_{mr} S} = 2\frac{g}{\pi\mu_{mr}(R^2 - r^2)} \tag{3}$$

Since the reluctance of the ferromagnetic path is neglected, the induction of the fluid can be considered as homogeneous along the gap. Considering a linear relationship between the magnetic field $H(t)$ and the magnetic flux density $B(t) = \mu_{mr} H(t)$, the magnetic field on the fluid is $H(t) = Ni(t)/\mu_{mr} S\mathscr{R}_d$. The relation between the magnetic

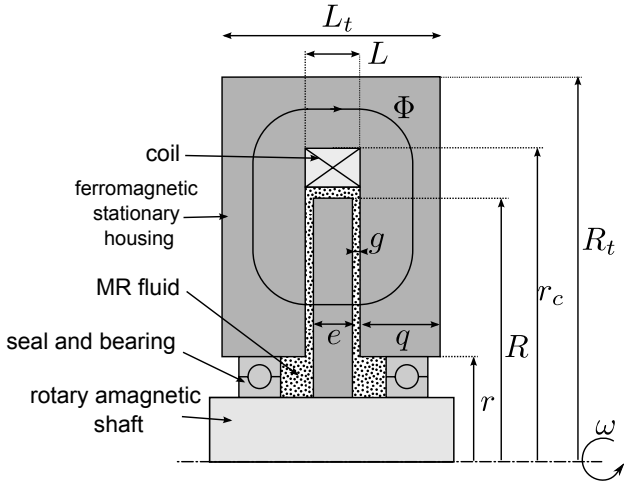

Fig. 3. Cross view of a single disc brake. An excitation coil, concentric to the axis, with an external radius r_c, generates the magnetic flux Φ. The fluid gap depth is noted g and the radius of the fluid gap are is R. The length of the disc and the gaps are called L and R_t and L_t are the external dimension of the brake taking into consideration all ferromagnetic paths. The total volume is $V_{td} = \pi R_t^2 L_t$. The velocity of the rotary shaft is denoted ω.

field and the field dependent yield stress $\tau(H)$ is typically denoted $\tau_z(H) = \alpha H(t)^\beta$ where α and β are two constant characteristics of the fluid [30]. Considering a linear behaviour ($\beta = 1$) and using the Bingham plastic model integrated over the active surface, the total controllable torque is $T_{maxd} = 4\pi(R^3 - r^3)N\alpha i_{max}/3S\mathscr{R}_d\mu_{mr}$.

The electromagnetic circuit is designed to develop a desired induction B_d over the fluid surface S. This value must be inferior to the saturation of the fluid. The torque, written as a function of B_d is:

$$T_{maxd} = \frac{4\pi}{3}(R^3 - r^3)\frac{\alpha}{\mu_{mr}} B_d \tag{4}$$

The necessary magnetic flux to achieve B_d is $\Phi = B_d S$. It defines the magneto-motive force $Ni = \Phi\mathscr{R}$ which can be correlated to the power supply. Calculated by Joule's losses, the power is $P = i^2 R_e$ where R_e is the electric resistance of the coil given by $R_e = 2\pi r_b \kappa N/S_w$ with κ the resistivity of the coil wire, r_b the mean radius of the coil, and S_w the section of the wire. Given a maximum current-to-surface ratio ν (A/m^2), the current is $i = S_w\nu$. Thus, the power as a function of Ni is $P = 2\pi r_b \nu\kappa Ni$.

With regard to B_d, the power is expressed as $P_{maxd} = 2\pi\kappa\nu r_b B_d S\mathscr{R}$. In the case of the single disc, it can be simplified to:

$$P_{maxd} = 4\pi\frac{1}{\mu_{mr}} r_b \kappa\nu g B_d \tag{5}$$

Considering only the reluctance of the fluid gap, the power supply of disc brake is indepent of the fluid surface length $(R - r)$.

The coil volume can be expressed as $V_{coil} = 2\pi r_b S_w N/\chi$ where χ is the coil fill rate. The volume of the coil as a function of the required power is $V_{coil} = P_{maxd}/\nu^2\kappa\chi$. Combining this expression with Equation (5) and considering that the coil width is $L = 2g + e$, where e is the width of a

disc, the external coi radius r_c can be deduced. Considering the coil as a RL circuit, the time constant proportional to the magnetic reluctance [51][55] is given by:

$$\delta t_c = \frac{N^2}{R_e \mathscr{R}_d} = \frac{S}{2\pi\kappa\nu r_b} B_d \tag{6}$$

Given the desired magnetic flux, in order to avoid saturation a minimal ferromagnetic path cross section S_{fer} has to be predicted, so that $S_{fer} = B_{fer}/\Phi$ where B_{fer} is the saturation point of the ferromagnetic material. This section can be refereed to the surface of the fluid. If we call $c_{sat} = B_d/B_{fer}$ the maximal induction ratio, the ferromagnetic section is $S_{fer} = c_{sat}S$, thus the ferromagnetic path and the fluid reach their saturation for the same flux. The minimal width q on both sides is $q = (R^2 - r^2)/2c_{sat}R$ and the minimal external radius R_t, taking into account the position of the coil is $R_t = \sqrt{(R^2 - q^2)c_{sat} + r_c^2}$. When the fluid surface and the desired field are defined, all other dimensions can be calculated. The total volume is $V_{td} = \pi R_t^2 L_t$ where R_t and L_t are the external radius and length. The volume is:

$$V_{td} = \pi[(R^2 - r^2)c_{sat} + r_c^2]\left[2g + e + \frac{(R^2 - r^2)c_{sat}}{r}\right] \tag{7}$$

Considering the fluid viscosity coefficient η and the rotational velocity $\omega(t)$, the viscous torque T_f is [30]:

$$T_f = 2\int_r^R \left(2\pi r_p^2\right)\left(\frac{\omega(t)\eta}{g} r_p\right) dr_p \tag{8}$$

Thus, the viscous torque coefficient $T_{vd} = T_f/\omega(t)$ is given by $T_{vd} = \pi\eta(R^4 - r^4)/g$.

The measures of performance can henceforth be determined. The global efficiency computed as $E_d = T_{max}/P_{max}$ is:

$$E_d = \alpha \frac{1}{3}\frac{(R^3 - r^3)}{g}\frac{1}{r_b\kappa\nu} \tag{9}$$

The efficiency is directly dependent on the fluid characteristics, on the gap depth and most notably, on the design of the coil. Equation (9) demonstrates also that the coil radius has to be as small as possible in order to minimize its electric resistance.

The reactivity is:

$$\delta t_d = \frac{8\pi}{3}\frac{\alpha}{\mu_{mr}} r_b\kappa\nu\frac{R^3 - r^3}{R^2 - r^2} \tag{10}$$

According to Equation (10), the reactivity depends on the fluid and on the coil design. The response time can be reduced by increasing the coil radius but it also increases the electric resistance and, as consequence, the power supply.

The torque density ρ_d is:

$$\rho_d = \frac{c_1(R^3 - r^3)}{[(R^2 - r^2)c_{sat} + r_c^2][2g + e + (R^2 - r^2)c_{sat}r^{-1}]} B_d \tag{11}$$

Where $c_1 = 4\alpha/3\mu_{mr}$. The controllability given by $K_d = T_{maxd}/T_{vd}$ can be expressed as follows:

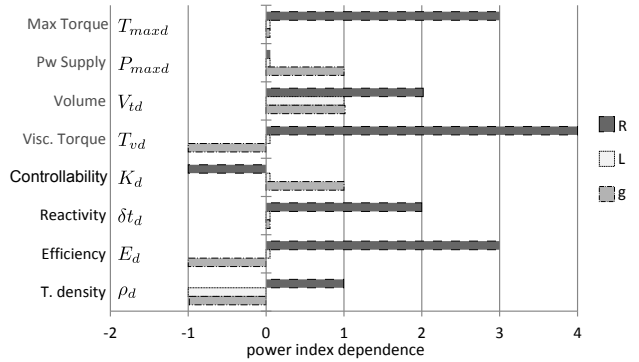

Fig. 4. Graphic representation of the evolution of the interdependent measure of performance as a function the dimensions. The coordinates of the graphic represent the highest polynomial power index of each criterion with regards to the radius R, length L and fluid gap depth g. For example, the efficiency depends on the cube of the radius, thus, it is represented by the index 3 with respect to the radius. .

$$K_d = \frac{4}{3}\frac{\alpha}{\mu\eta} g\frac{(R^3 - r^3)}{(R^4 - r^4)} B_d \tag{12}$$

Equation (12) shows that K is proportional to the gap depth, inversely proportional to the radius and depends on the fluid characteristics. A large gap generates less viscous torque but increases the power. Fig. 4 presents a graphic representation of the evaluation criteria as a function of the dimensions.

For a disc brake, only the fluid surface radius and the gap are necessary to design a brake with optimizated torque density. Increasing the radius improves the efficiency, the resistivity and the maximal torque. However, the viscous torque increases faster, reducing the controllability. The radius sets the controllability/torque tradeoff. The length Lhas no effect on the performance since the reluctance of the ferromagnetic path is neglected. For a given power, a small fluid gap g provides high maximal torque but the viscous torque increases too. The gap depth then governs a tradeoff between the controllability and maximal torque. Nevertheless, large gaps provide low zero-field torque but the power increases. The gap defines also the tradeoff between controllability and efficiency.

For brakes with large L/R ratio, the design tends to cylindrical brakes. This corresponds to the second basic geometry presented in the following section.

3.2 Cylinder-Shaped Brakes

The second elementary brake has a cylindrical shaped geometry and are also called drum-brakes. A schematic cross view is presented in Fig. 5.

If R is the fluid gap radius and r is the radius of the inner section crossed by the flux, the reluctance is given by the integral of the reluctance of fluid gap from the cylinder R up to $R + g$ along the radius du computed as:

$$\mathscr{R}_c = \int_R^{R+g} \frac{2}{\mu_{mr}(2\pi R(L - h))} du = \frac{ln(1 + \frac{g}{R})}{\pi\mu_{mr}(L - h)} \tag{13}$$

Where h is the height of the coil. Considering $R >> g$, the reluctance can be satisfactorily approximated as $\mathscr{R}_c =$

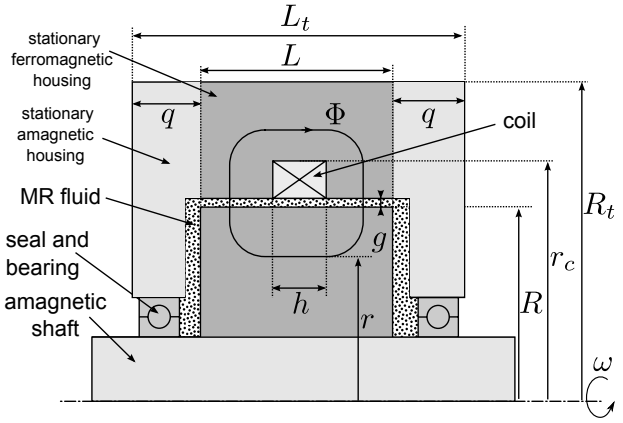

Fig. 5. Single drum brake. The radius and length of the fluid gap are called R and L. The inner radius is called r. An excitation coil with external radius r_c and height h provides the magnetic flux Φ. The active surface is $2\pi R(L-h)$. The magnetic flux is supposed to be homogeneous along the fluid gap g and the total volume is $V_{tc} = \pi R_t^2 L_t$. The rotary shaft velocity is ω. The width of the lateral supports is denoted q.

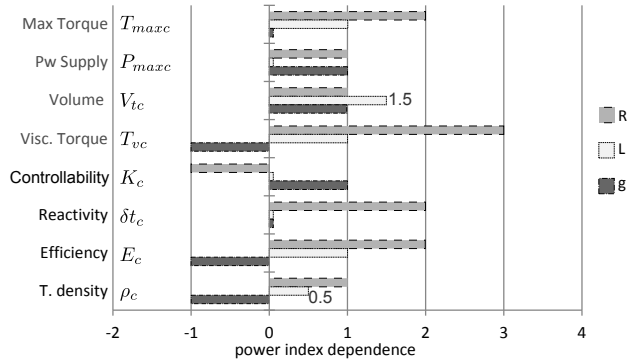

Fig. 6. Cylindrical brake performance as a function of its external dimension

$g/\left[\pi\mu_{mr}(L-h)R\right]$. Combining equation 2 with the equation of the induction on the fluid, the controllable torque is $T_{maxc} = 2\pi R^2(L-h)\alpha Ni/S\mathscr{R}_c\mu_{mr}$, which can be rewritten as a function of B_d as:

$$T_{maxc} = 2\pi R^2(L-h)\frac{\alpha}{\mu_{mr}}B_d \tag{14}$$

By contrast to disc-brakes, the maximal torque is proportional to the length. The necessary power P_{maxc} is obtained using the same procedure employed for the disc-type. The efficiency is $E_c = T_{maxc}/P_{maxc}$, expressed as:

$$E_c = \alpha\frac{1}{2}\frac{R^2(L-h)}{g}\frac{1}{r_b\kappa\nu} \tag{15}$$

Considering only the fluid surface and $R >> g$, the viscous torque can be approximated by Equation (16) [58]. A complete viscous model can be found in[34].

$$T_f = \int_0^{2\pi}\int_0^{L-h} R\tau d\theta dS = \int_0^{L-h} R\frac{\eta R\omega(t)}{g}2\pi R dl \tag{16}$$

Thus, the viscous torque to velocity coefficient is $T_{vc} = 2\pi\eta(L-h)R^3/g$. The viscous torque depends on the cylinder radius and on the fluid gap depth. The controllability $K_c = T_{maxc}/T_{vc}$ is computed as:

$$K_c = \frac{\alpha}{\mu_{mr}\eta}\frac{g}{R}B_d \tag{17}$$

The controllability is proportional to the fluid gap, inversely proportional to the radius and independent of the length L. Thus, in order to improve T_{maxc} without altering the controllability, the length should be increased instead of the radius.

The required section on the top of the coil and below the fluid gap is $S_{fe} = 2\pi c_{sat} r\,(L-h)$. This gives a total radius $R_t = \sqrt{c_{sat}R\,(L-h) + r_c^2}$, where r_c is the coil radius which can be determined using the coil volume. The required inner radius to avoid saturation is $r = \sqrt{R^2 - c_{sat}R\,(L-h)}$. Note that the inner radius specifies the maximal length of the fluid gap.

The volume of the brake is $V_{tc} = \pi L_t R_t$ and the torque density $\rho_c = T_{maxc}/V_{tc}$ is:

$$\rho_c = \frac{\alpha}{\mu_{mr}}\frac{2R^2(L-h)}{[c_{sat}(L-h)R + r_c^2](2q+e)}B_d \tag{18}$$

The time constant is obtained combining Equation (6) with Equation (13), and is given by $\delta t_r = B_d(L-h)R/\left[2\kappa\nu r_b\right]$. The reactivity, in terms of Nm/s, is:

$$\delta t_c = 4\pi\kappa\nu r_b R\frac{\alpha}{\mu_{mr}} \tag{19}$$

Fig. 6 presents the evolution of all parameters as a function of L and R. Increasing the radius improves the maximal torque, the efficiency, and the reactivity but the controllability decreases. The length L plays an important role on the efficiency and maximal torque. The same tradeoffs between torque and controllability and between reactivity and power are observed.

3.3 Finite Element Modelling

The magnetostatic models have been simulated using finite element analysis (FEA). The FEA uses FEMM[1] software. The model is solved with the same geometry in Matlab and with the FEA software. The fluid is Lord Corp. MFR-122EG [57]. In the analytical model, are considered as constant: $B_d = 0.7$T, $\eta = 0.1$Pa.s, $\alpha = 0.22$Pa.m/A, $\mu_{mr} = 24\pi 10^{-7}$A/m and $B_{fer} = 1.4$T. In the FEA, the B-H curves (flux density *vs* magnetic field) of the fluid and the ferromagnetic path (Telar 57S), are given by the manufacturer's specifications. The same procedure is employed to obtain the variable $\alpha(H)$ (magnetic field to yield stress constant). For the coil design consider: $\nu = 6$A/mm^2, $\kappa = 17.10^{-9}\Omega m$, $S_w = 4,9.10^{-8}$m^2 and $\chi = 70\%$.

Only three variables need to be specified: the desired magnetic flux density B_d, the fluid gap g and its radius R. All other dimensions can optimally be deduced. The fluid gap is 0.5mm. The radius varies from 10mm to 170mm for the cylinder brake and from 10mm to 250mm for the disc brake in order to achieve equivalent volumes.

[1]Finite Element Method Magnetics: www.femm.info

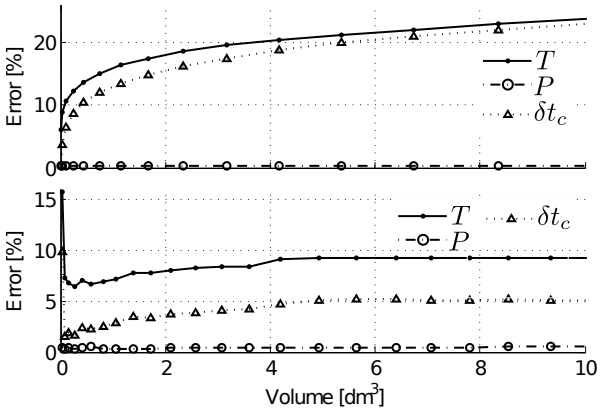

Fig. 7. Relative error between the analytical model and FEA for the single disc (top) and the single cylinder brake (bottom). Where T, P and δt_c are the torque, the power, and the time constant respectively.

The relative error between the analytical model and the FEA as a function of the brake volume is presented in Fig. 7. The difference in terms of power is less than 0.5%. The reluctance obtained in the analytical model is inferior than with the FEA, which directly affects the response time, (given by Equation 10). Considering the power calculated in the analytical model, the magnetic flux in the FEA is not sufficient to achieve B_d, reducing the maximal torque. For the disc and the cylindrical brakes, the maximal torque error is 23% and 9.8% respectively, and in terms of response time, the error is 23% and 8.7%. These differences correpond however to a volume of 10dm^3 (a cube with 373mm space diagonal or a 500mm diameter disc brake) which is rarelly the case of an MR brake .

The error increases with the brake volume. If the FEA neglects the reluctance of the ferromagnetic path, the error is reduced to 3.1% and 1.9% for the torque and less than 1% for time constant. The error depends also on the fluid gap depth. For example, for g=0.3mm, the torque error for the disc and for the cylinder rises to 31.1% and 13.8%, for g=0.75mm, this is reduced to 18.8% and 6.5%.

The maximal magnetic flux density observed in the ferromagnetic path is 1.38T. As predicted by the model, the ferromagnetic path is maintained under the saturation point of the material.

3.4 Discussion

The FEA simulation results for each brake are presented in Fig. For the cylinder brake, the lateral support are arbitrary fixed to $q = 2$mm. 8. Both brakes exhibits an equivalent torque density for a given volume. The results show that disc brakes possess better efficiency than drum brakes and generate less viscous friction. Conversely, drum brakes react faster.

The proposed model allows for an optimal design of both brake types in term of torque density. Oonly the fluid surface and the desired flux density should be specified. The other dimensions can be calculated to provide the required flux and to avoid the saturation of the ferromagnetic path.

For disc brakes, when the radius R is defined, an optimal length L_t can be calculated to support the magnetic flux so that $L_t = c_{cat}(R^2 - r^2)/R + 2g + e$. The minimum outer

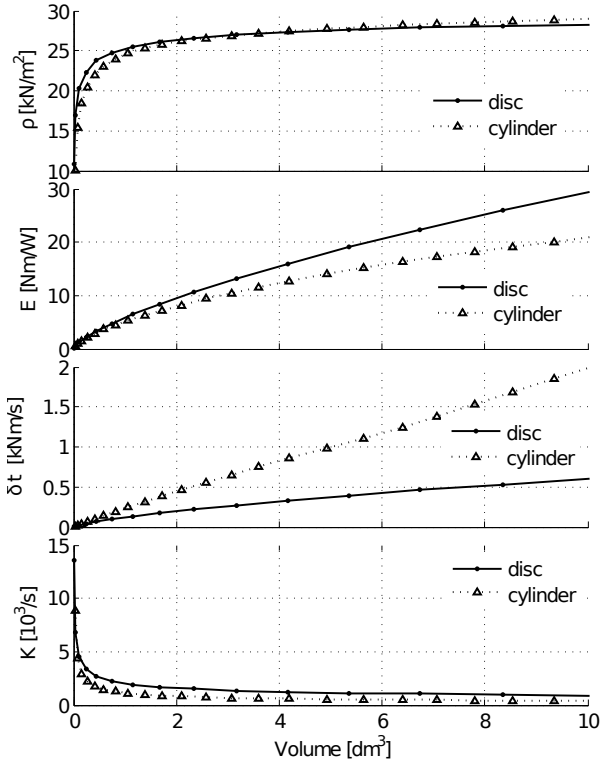

Fig. 8. Measures of performance as a function of the volume by FEA. The results present the optimised torque density ρ for a given L_t/R_t ratio. The efficiency E is higher in a disc brake for L_t/R_t <0.48 but the reactivity δt is inferior than cylinder brakes. Disc brakes present higher controllability K.

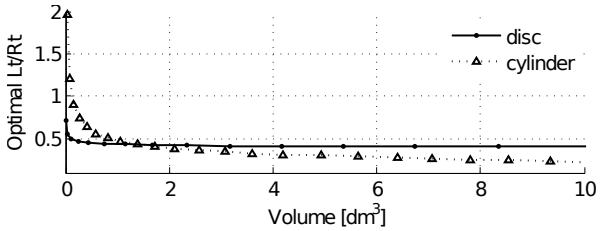

Fig. 9. Optimal L_t/R_t ratios for single disc and single cylinder brakes as a function of the external volume.

radius R_t necessary to accommodate the coil is a function of R. For a cylinder brake, the relation length/radius is $L_t = (R^2 - r^2)/2Rc_{cat} + h + 2q$. Therefore, for a given volume, there is an optimal L_t/R_t ratio that minimizes the volume and as a consequence maximises the torque density.

The optimal L_t/R_t ratios are presented in Fig. 9. In the volume range of 0.03dm^3 to 10dm^3, the optimal ratio for a disc brake varies from 0.40 to 0.72 and for a cylinder brake from to 0.21 to 1.96. This highlights that optimal disc brakes present external flat forms while cylinder brakes can take more varied forms. The choice of brake design then depends on the available volume and the volume form. The measures of performance as a function of the L_t/R_t ratios are shown in Fig. 10. For large L_t/R_t, drum brakes provide more torque density, since the length in a disc brake has no influence on the torque but affects the volume.

The model of the controllable and viscous torque suggests that in the case of a cylinder brake, there is an unwanted torque

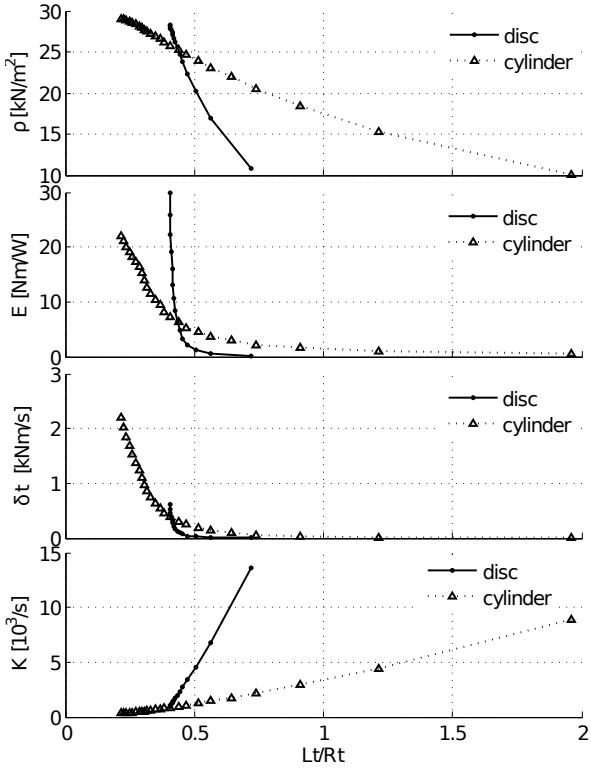

Fig. 10. Measures of performance as a function of the L_t/R_t ratio. The results present the maximal torque density that can be achieved for a geometrical form.

jump during the transition from $B_d = 0$ to $B_d \neq 0$. As shown in [59], for the disc brake this torque jump can be avoided by properly choosing r and R.

In order to improve the maximal torque, several fluid gaps can be combined in parallel. Section 4 investigates the performance of both brakes types in this case.

4. Multiple-Layered Brakes

We turn now our focus to the design of brakes comprising multiple cylinders or discs in parallel.

4.1 Multiple-Disc Based Brakes

A schematic representation of a multiple disc brake is shown in Fig. 11. Consider m the number of fluid gaps. Note that a disc has two fluid gape. The thickness L depends on the number of gaps, so that $L = gm + e(m-1)$.

The total reluctance is expressed as a sum of the reluctance $\mathscr{R}_d$ of a single disc k, presented by Equation (3), as:

$$\mathscr{R}_{md} = \mathscr{R}_d \frac{m}{2} \tag{20}$$

The torque T_{md} of a mutiple disc, expressed as a function of the torque of a single disc T_{maxd} and the number of fluid gaps is:

$$T_{md} = T_{maxd} \frac{m}{2} \tag{21}$$

The necessary power supply P_{md} to achieve this torque, if only the reluctance of the fluid is considered is:

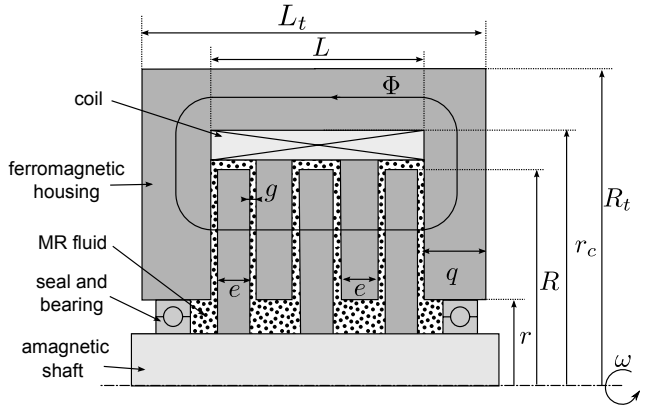

Fig. 11. Multiple-Layered disc-based brake comprising three elementary discs and six gaps ($m = 6$) in parallel. Each disc k possesses an inner radius r, a fluid gap radius R and a thickness e. A coil with a mean radius r_b generates the flux Φ. The total radius and length are denoted R_t and L_t.

$$P_{md} = P_{maxd} \frac{m}{2} \tag{22}$$

It can be concluded that the efficiency E_{md} of the brake is independent of the number of fluid gaps. The viscous torque coefficient T_{vmd} is given by:

$$T_{vmd} = T_{vd} \frac{m}{2} \tag{23}$$

Thus, the controllability K_{md} is independent of the number of fluid gaps.

The volume of the brake is $V_{md} = \pi R_t^2 L_t$ where the total length is defined as $L_t = c_{cat}(R^2 - r^2)/R + mg + e(m-1)$ and $R_t = \sqrt{c_{sat}(R^2 - r^2) + r_c^2}$. The torque density ρ_{md} is:

$$\rho_{md} = \frac{c_2(R^3 - r^3)}{[L + (R^2 - r^2)c_{sat} r_c^{-1}][(R^2 - r^2)c_{sat} + r_c^2]} m B_d \tag{24}$$

With $c_2 = 2\alpha/3\mu_{mr}$ and $L = gm + e(m-1)$. The torque density is proportional to the number of fluid gaps. Finally, the reactivity as a function of the reactivity of a single disc is:

$$\delta t_{md} = \delta t_d \frac{m}{2} \tag{25}$$

The evolution of all measures of performance as a function of the number of fluid gaps is synthesized in Fig.12. The reactivity and the torque density increase with m. The efficiency and controllability remain constant.

4.2 Multiple-Cylinder Based Brake

Consider the multiple-cylinder brake presented in Fig. 13. The external radius of the fluid chamber R is proportional to the number of fluid gaps. The relation between all measure of performance and the number of gaps is non-linear.

The radius R of the largest fluid surface as function of number of fluid gaps m is $R = r + gm + e(m-1)$ where r is the radius of the smallest one. The surface of each fluid gap k is $S_k = 2\pi L r_k^2$ where $r_k = r + (k-1)(e+g)$. Thus, the reluctance can be calculated by:

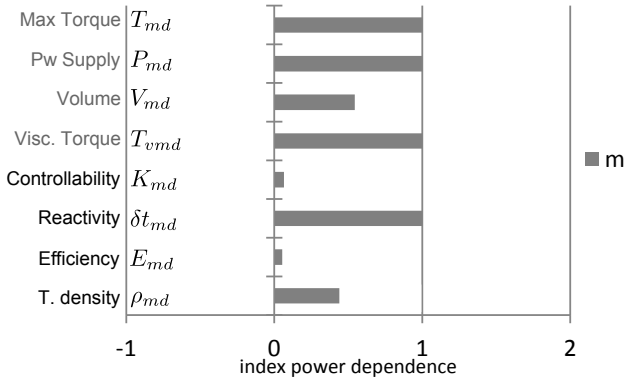

Fig. 12. Multilayered disc brake performance as a function of the number of fluid gaps

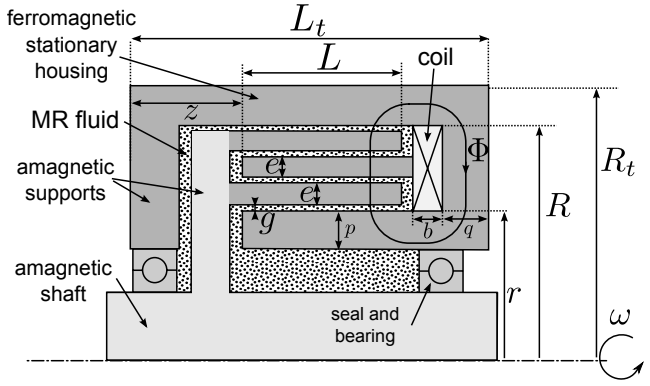

Fig. 13. Multiple cylinder brake with m fluid gaps: the radius of the smallest and largest fluid surface are r and R. The external length and radius are L_t and R_t. Each cylinder k separated by a gap g has a thickness e, a radius r_k and length L. The width of the coil and of the path on its right side are b and q. The thickness of the path below the smallest fluid surface is p and z is the width of the lateral supports. The velocity of the shaft is ω.

$$\mathscr{R}_{mc} = \frac{1}{2\pi\mu_{mr}L}\int_r^R \frac{dr}{r} = g\frac{ln\left(1+m\frac{e+g}{r}\right)}{2\pi\mu_{mr}L(g+e)} \qquad (26)$$

For a given magnetic flux, the smallest surface saturates before the others. Thus, the magnetic circuit is designed to provide the desired induction B_d over this surface. The controllable torque is the sum of the torque provided by each cylinder and can be expressed as a function of B_d as :

$$T_{mc} = 2\pi r^2 L\frac{\alpha}{\mu_{mr}}\left[m + \frac{(m-1)(R-r)}{2r}\right]B_d \qquad (27)$$

Note that if $m = 1 \therefore r = R$, therefore the torque collapses to the single cylinder. Replacing the reluctance in Equation (5), the power is given by:

$$P_{mc} = \pi\frac{\nu\kappa}{\mu_{mr}}\frac{(r+R)rg}{e+g}ln\left(1+\frac{m(e+g)}{r}\right)B_d \qquad (28)$$

Increasing the number of fluid gaps requires more power supply. The coil width b can be deduced from the coil volume so that $b = P_{mc}/\pi(R^2-r^2)\nu^2\kappa\chi$ or clearer: $b = gB_d(R-r)ln[1+(e+g)r^{-1}]/\nu\mu_{mr}(e+g)(R^2-3r^2)$. The efficiency $E_{mc} = T_{mc}/P_{mc}$ yields:

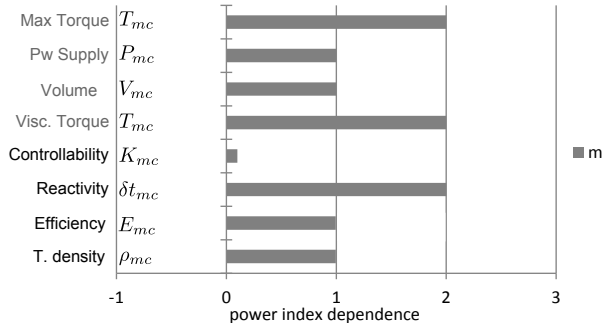

Fig. 14. Measure of performance of a multiple cylinder brake as a function of the number of fluid gaps m.

$$E_{mc} = \frac{\alpha}{\nu\kappa}\frac{L(e+g)[2rm+b(m-1)]}{g(2r+R-r)ln\left[1+m(e+g)r^{-1}\right]} \qquad (29)$$

This equation demontrates that the efficiency increases with the number of fluid gaps. The viscous torque coefficient, as the sum of the torque of each cylinder is $T_{vmc} = 2\pi\frac{\eta L}{g}\sum_{k=1}^{m}\left[r+(k-1)(e+g)\right]^3$. This expression can be approximated by:

$$T_{vmc} = 2\pi\frac{\eta L r^3}{g}\left[1+\frac{3}{2}(\frac{e+g}{r})(m-1)\right]m \qquad (30)$$

Subsequently, the controllability is obtained by:

$$K_{mc} = \frac{\alpha}{\mu\eta}\frac{g}{r}\left[\frac{2r+(m-1)(e+g)}{2r+3(m-1)(e+g)}\right]B_d \qquad (31)$$

The minimal external radius, taking into consideration the saturation of the path on the top of the coil, is $R_t = \sqrt{2rLc_{sat}+R^2}$. The width on the right side of the coil is $q = Lc_{sat}$. Assumig that the lateral support z has the same width q of the magnetic path, the total length is $L_t = 2q+L+b$. The torque density is calculated as:

$$\rho_{mc} = \frac{\alpha}{\mu_{mr}}\frac{rL[2rm+(m-1)(R-r)]}{(2rLc_{sat}+R^2)[L(2c_{sat}+1)+b]}B_d \qquad (32)$$

The analysis of this equation demonstrates that the torque density increases with the number of fluid gaps. Finally, the time constant is $\delta t_c = 2RLB_d/\nu\kappa(2R+L)$. The reactivity is computed as follows:

$$\delta t_{mc} = \pi\frac{\alpha\nu\kappa}{\mu_{mr}}r(R-r)\left[m+\frac{(m-1)(R-r)}{2r}\right] \qquad (33)$$

Since the reluctance increases with the number of gaps, the time constant time decreases and the reactivity is improved. Fig. 14 presents a synthesized representation of the measures of performance as a function of m. Increasing the number of fluid gaps improves the efficiency, reactivity and torque density.

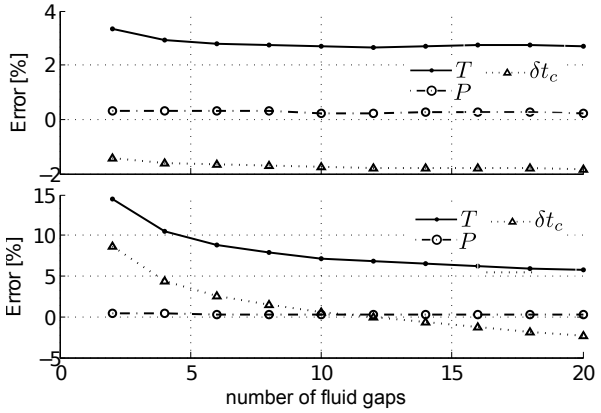

Fig. 15. Relative error between the analytical model and the FEA for the mutiple disc (top) and the multiple cylinder brake (bottom) as a function of the number of fluid gaps. Where T, P and δt_c is the torque, the power and the time constant respectively.

4.3 Finite Element Modelling

Both brakes have been evaluated using FEA. The characteristics of the coil, of the fluid and of the ferromagnetic material are the same that those employed in the previous section. In the case of disc brakes, the inner radius is arbitrary fixed to R =50mm, and for cylinder brakes r =35mm. The maximal length of the fluid gap is $L = r/2c_{sat}$. In both cases, the width of a cylinder and a disc is e=1mm. The number of fluid gaps m varies from 2 to 20.

The relative error between the analytical model and the FEA is presented in Fig. 15. For disc brakes, the relative error can be assumed as constant regardless the number of gaps. For the multiple cylinder, the power error is constant while in terms of torque, it decreases with m. In both cases, the error increases with the brake volume.

4.4 Discussion

The multiple layered brake models demonstrate that the association of many elementary cylinders or discs in parallel is an effective way to improve the global performance, in particular the torque density.

The addition of these repetitions gives to the model an additional parameter: In the case of a multiple disc brake, the radius, the fluid gap depth and the number of fluid gaps are the geometrical model inputs. All other dimensions can be calculated accordingly. The length of the brake is proportional to m. The torque density is therefore proportional to the radius and the number of fluid gaps. The measures of performance are listed in Fig. 16.

For multiple cylinder brakes, the model input are the radius of the smallest fluid surface r, the fluid gap depth and the number of fluid gaps m. The length L of the fluid surface can be determined in order to optimize the torque density and depends on the radius, so that $L < rc_{sat}$. The measures of performance are presented in Fig. 17.

For a maximal number of fluid gaps of 20, the obtained L_t/R_t ratio is given in Fig. 18. When the number of fluid gaps is constant, the evolution of the measure of performance is similar to a single cylinder brake.

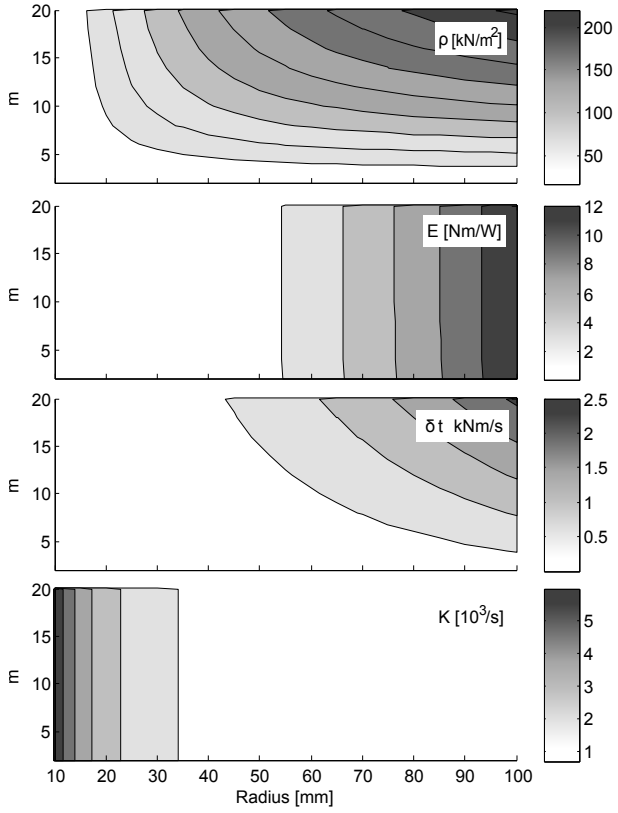

Fig. 16. Multiple disc brake performance as a function of the number of fluid gaps m and the radius of the fluid gap R. The torque density ρ and the reactivity δt are proportional to the number of fluid gaps while the controllability K and the efficiency E are independent of m.

In next the section, the influence of the fluid characteristics is addressed.

5. Influence of the MR fluid and Materials

Whether for disc or cylinder brakes, the influence of some intrinsic parameters of the fluid and the housing materials is the same. Generally, performance are improved if the fluid has a high field to yield stress constant α and low viscosity η. However, in available commercial MR fluids, α and η are linked to the ferromagnetic particle density. As a consequence the choice of a fluid establishes some compromises, in particular between the maximum torque and zero-field torque.

The power supply increases with the reluctance while the time constant in inversely proportional to it. Therefore, the relative permeability μ_{mr} of the fluid and of the ferromagnetic path has a dual effect: an increasing-permeability reduces the power supply but reduces also the reactivity of the brake. The material should posses a high permeability (or low reluctance) to properly guide and focus the magnetic flux into the MR fluid gap and minimize flux leakages. Furthemore, the power supply is proportional to the reluctance observed by the coil, thus high permeability reduces the volume of the coil and the volume of the brake.

The influence the fluid properties and of the permeability of the ferromagnetic path is presented in Fig. 19.

In the proposed model, the magnetic circuit is designed to provide B_d over the fluid surface. This field can correspond

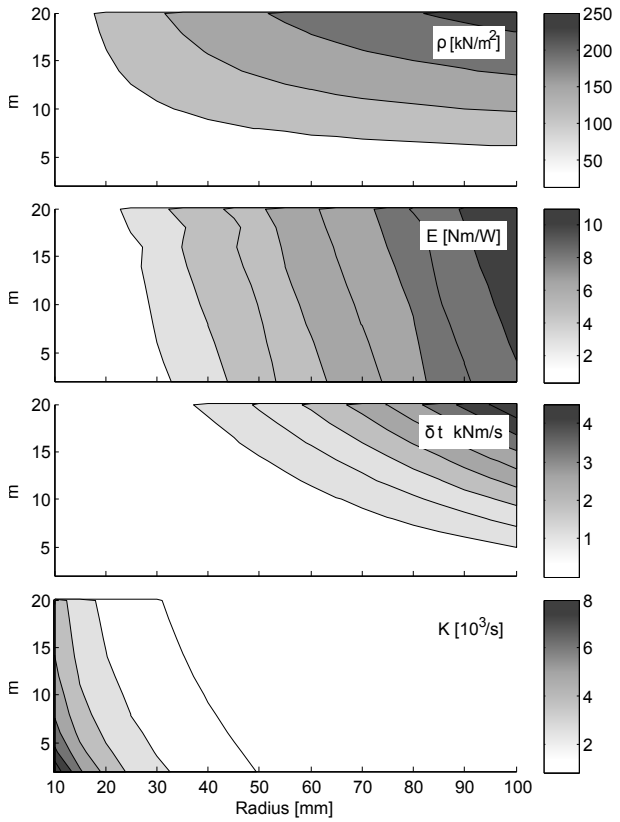

Fig. 17. Multiple cylinder brake performance as a function of the number of fluid gaps m and the radius R of the smallest fluid surface. The torque density ρ, the efficiency E and the reactivity δt increases with m while the controllability K monotonically decreases.

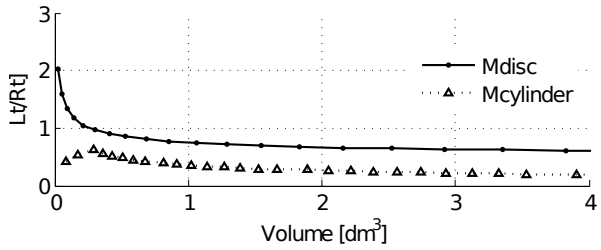

Fig. 18. Obtained geometric form as a function of the volume for 20 fluid gaps.

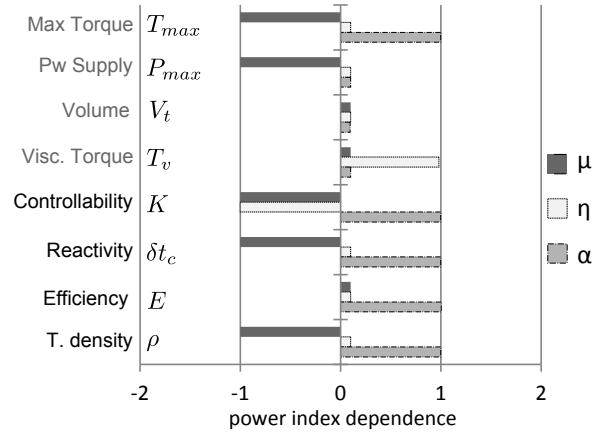

Fig. 19. Influence of fluid intrinsic parameters in the performance. The magnetic permeability of the magnetic circuit, the viscosity coefficient and the field-to-yield stress constant are μ, η , and α respectively .

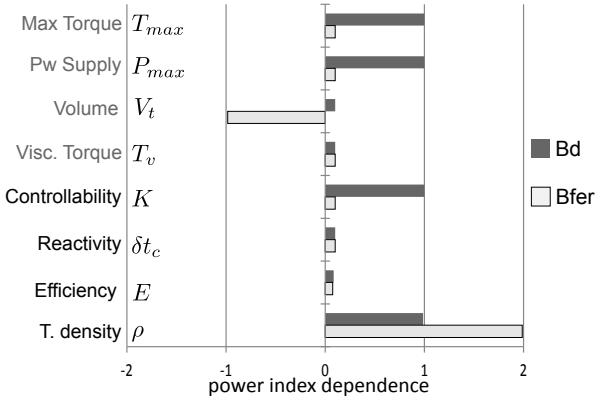

Fig. 20. Influence of the maximal admissible inductions of the fluid and of the housing material on the brake performance.

to the saturation point of the fluid which bounds the linear range of the brake. The torque density is improved if B_d is increased as presented in Fig. 20. The maximal admissible induction of the housing material B_{fer} affects only the brake volume, and as a consequence, the torque density. A high B_{fer} allows for the minimization of the ferromagnetic path as well as the width of ferromagnetic cylinder or discs.

6. Conclusion

The proposed model is specified to provide a required induction over the fluid surface. When its radius and the gap depth are defined, the power and all other dimensions can be deduced. It can be concluded that all evaluation criteria are interdependent.

The length of a single disc brake has no considerable influence on its performance while increasing the radius improves the efficiency, the reactivity and the torque density. The results highlight that to improve torque density, a disc brake is adaptable for external dimensions ratio between 0.4 and 0.72. By contrast, for a single drum brake, both the length and the radius have an influence on the performance. The torque density and efficiency are proportional to them. Given a radius, the optimal length of the fluid gap can be determined to improve torque density. The external dimensions are connected but the brake can assume more different forms than disc brakes (0.21 to 1.96 for a volume inferior to 10dm^3).

In an optimal configuration, the results demonstrate that both brakes exhibit equivalent torque density for a given volume. Drum brakes however are more reactive but need more power than disc brakes. For high L_t/R_t ratios, drum brakes have higher torque density. FEA has been used to strengthen the models. The error between the model and the FEA is proportional to the volume. For an uncommon volume of 10dm^3 the torque difference attains 23% and 9% for a disc and a cylinder brake respectively.

For multiple-layered brakes, the maximal torque, the torque density and the reactivity rise with the number of fluid gaps. The controllability and the efficiency remain constant. The performance depends also on the brake radius, which should be specified and follows the same dependence as presented for single brakes. The fluid gap depth has an important role. Large

gaps require high power supply and large coil volume while the viscous torque is reduced. The fluid gap depth represents the compromise between controllability and efficiency.

The choice of a brake type remains dependent on the application and on the compromises between the different measures of performance.

REFERENCES

[1] E. Gedik, H. Kurt, Z. Recebli, and C. Balan, "Two-dimensional cfd simulation of magnetorheological fluid between two fixed parallel plates applied external magnetic field," *Computers & Fluids*, 2012.

[2] S. Melle and J. E. Martin, "Chain model of a magnetorheological suspension in a rotating field," *The Journal of Chemical Physics*, vol. 118, no. 21, pp. 9875–9881, 2003.

[3] C. Rossa, J. Lozada, and A. Micaelli, "Magnetic flux analysis on magnetorheological actuators can detect external force variation," in *Sensors, 2012 IEEE*, 2012, pp. 1–4.

[4] W. H. Li, H. Du, G. Chen, S. H. Yeo, and N. Q. Guo, "Nonlinear rheological behavior of magnetorheological fluids: step-strain experiments," *Smart Materials and Structures*, vol. 11, no. 2, p. 209, 2002.

[5] M. R. Jolly, J. W. Bender, and J. D. Carlson, "Properties and applications of commercial magnetorheological fluids," in *Smart Structures and Materials*, L. P. Davis, Ed., vol. 3327. SPIE, 1998, pp. 262–275.

[6] G. Bossis, S. Lacis, A. Meunier, and O. Volkova, "Magnetorheological fluids," *Journal of Magnetism and Magnetic Materials*, vol. 252, pp. 224 – 228, 2002, proceedings of the 9th International Conference on Magnetic Fluids.

[7] N. Mohammadi, M. Mahjoob, B. Kaffashi, and S. Malakooti, "An experimental evaluation of pre-yield and post-yield rheological models of magnetic field dependent smart materials," *Journal of Mechanical Science and Technology*, vol. 24, pp. 1829–1837, 2010, 10.1007/s12206-010-0607-x.

[8] C. Rossa, L. Eck, A. Micaelli, and J. Lozada, "On a novel torque detection technique for magnetorheological actuators," *Sensors Journal, IEEE*, vol. PP, no. 99, pp. 1–1, 2013.

[9] D. Lee and N. M. Wereley, "Analysis of electro- and magneto-rheological flow mode dampers using Herschel-Bulkley model," *Proceedings of SPIE*, vol. 3989, no. 1, pp. 244–255, Apr. 2000.

[10] J. Lindler and N. M. Wereley, "Quasi-steady bingham plastic analysis of an electrorheological flow mode bypass damper with piston bleed," *Smart Materials and Structures*, vol. 12, no. 3, pp. 305–317, Jun. 2003.

[11] J. Carlson and M. R. Jolly, "Mr fluid, foam and elastomer devices," *Mechatronics*, vol. 10, pp. 555 – 569, 2000.

[12] A. Olabi and A. Grunwald, "Design and application of magneto-rheological fluid," *Materials & Design*, vol. 28, no. 10, pp. 2658–2664, 2007.

[13] J. Z. Chen and W. H. Liao, "Design, testing and control of a magnetorheological actuator for assistive knee braces," *Smart Materials and Structures*, vol. 19, no. 3, p. 035029, 2010.

[14] P. Fauteux, M. Lauria, M.-A. Legault, B. Heintz, and F. Michaud, "Dual differential rheological actuator for robotic interaction tasks," in *Advanced Intelligent Mechatronics, 2009. AIM 2009. IEEE/ASME International Conference on*, july 2009, pp. 47 –52.

[15] H. J., Z. J.Q., Y. Y., and W. Y.Q., "Analysis and design of a cylindrical magneto-rheological fluid brake," *Journal of Materials Processing Technology*, vol. 129, no. 1, pp. 559–562, 2002.

[16] F. Periquet and J. Lozada, "A miniature 1-dof mr fluid based haptic interface," in *nternational Exhibition on Smart Actuators and Drive Systems*, 2010.

[17] H. X. Ai, D. H. Wang, and W. H. Liao, "Design and modeling of a magnetorheological valve with both annular and radial flow paths," *Journal of Intelligent Material Systems and Structures*, vol. 17, no. 4, pp. 327–334, Jan. 2006.

[18] T. Saito and H. Ikeda, "Development of normally closed type of magnetorheological clutch and its application to safe torque control system of Human-Collaborative robot," *Journal of Intelligent Material Systems and Structures*, vol. 18, no. 12, pp. 1181–1185, Jan. 2007.

[19] S. J. Dyke, B. F. S. Jr, M. K. Sain, and J. D. Carlson, "An experimental study of mr dampers for seismic protection," *Smart Materials and Structures*, vol. 7, no. 5, p. 693, 1998.

[20] Y. F. Duan, Y. Q. Ni, and J. M. Ko, "Cable vibration control using magnetorheological dampers," *Journal of Intelligent Material Systems and Structures*, vol. 17, no. 4, pp. 321–325, Jan. 2006.

[21] T. Kikuchi, K. Oda, and J. Furusho, "Leg-robot for demonstration of spastic movements of Brain-Injured patients with compact magnetorheological fluid clutch," *Advanced Robotics*, vol. 24, no. 5-6, pp. 671–686, 2010.

[22] J. Chen and W. Liao, "A leg exoskeleton utilizing a magnetorheological actuator," in *Robotics and Biomimetics, 2006. ROBIO '06. IEEE International Conference on*, 2006, pp. 824 –829.

[23] C. Rossa, J. Lozada, and A. Micaelli, "A new hybrid actuator approach for force-feedback devices," in *Intelligent Robots and Systems (IROS), 2012 IEEE/RSJ International Conference on*, 2012.

[24] J. Blake and H. Gurocak, "Haptic glove with mr brakes for virtual reality," *Mechatronics, IEEE/ASME Transactions on*, vol. 14, no. 5, pp. 606 –615, oct. 2009.

[25] J. Lozada, M. Hafez, and X. Boutillon, "A novel haptic interface for musical keyboards," in *Advanced intelligent mechatronics, 2007 IEEE/ASME international conference on*, sept. 2007, pp. 1 –6.

[26] C. Rossa, J. Lozada, and A. Micaelli, "Stable haptic interaction using passive and active actuators," in *Robotics and Automation (ICRA), 2013 IEEE International Conference on*, 2013, pp. 2386–2392.

[27] T. Kikuchi and K. Kobayashi, "Development of cylindrical magnetorheological fluid brake for virtual cycling system," in *Robotics and Biomimetics (ROBIO), 2011 IEEE International Conference on*, Dec. 2011, pp. 2547 –2552.

[28] C. Rossa, J. Lozada, and A. Micaelli, "Interaction power flow based control of a 1-dof hybrid haptic interface," in *Proceedings of the 2012 international conference on Haptics: perception, devices, mobility, and communication - Volume Part II*, ser. EuroHaptics'12. Berlin, Heidelberg: Springer-Verlag, 2012, pp. 151–156.

[29] A. J. McDaniel, "Magneto-rheological brake-clutch apparatuses and methods," Feb. 2011, U.S. Classification: 192/12.00A.

[30] W. Li and H. Du, "Design and experimental evaluation of a magnetorheological brake," *The International Journal of Advanced Manufacturing Technology*, vol. 21, no. 7, pp. 508–515, 2003.

[31] W. Li, B. Liu, P. Kosasih, and X. Zhang, "A 2-dof mr actuator joystick for virtual reality applications," *Sensors and Actuators A: Physical*, vol. 137, no. 2, pp. 308 – 320, 2007.

[32] K. Karakoc, E. J. Park, and A. Suleman, "Design considerations for an automotive magnetorheological brake," *Mechatronics*, vol. 18, no. 8, pp. 434–447, Oct. 2008.

[33] B. Assadsangabi, F. Daneshmand, N. Vahdati, M. Eghtesad, and Y. Bazargan-Lari, "Optimization and design of disk-type MR brakes," *International Journal of Automotive Technology*, vol. 12, no. 6, pp. 921–932, 2011.

[34] J. Huang, J. Zhang, Y. Yang, and Y. Wei, "Analysis and design of a cylindrical magneto-rheological fluid brake," *Journal of Materials Processing Technology*, vol. 129, no. 1–3, pp. 559–562, Oct. 2002.

[35] Y. J. Shiao and C. Y. Chang, "Design of an innovative High-Torque brake," *Advanced Materials Research*, vol. 339, pp. 84–87, Sep. 2011.

[36] M. Avraam, M. Horodinca, P. Letier, and A. Preumont, "Portable smart wrist rehabilitation device driven by rotational MR-fluid brake actuator for telemedecine applications," in *Intelligent Robots and Systems, 2008. IROS 2008. IEEE/RSJ International Conference on*, Sep. 2008, pp. 1441 –1446.

[37] N. C. Rosenfeld and N. M. Wereley, "Volume-constrained optimization of magnetorheological and electrorheological valves and dampers," *Smart Materials and Structures*, vol. 13, no. 6, pp. 1303–1313, Dec. 2004.

[38] Q. H. Nguyen and S. B. Choi, "Optimal design of a novel hybrid MR brake for motorcycles considering axial and radial magnetic flux," *Smart Materials and Structures*, vol. 21, no. 5, p. 055003, May 2012.

[39] H. Nguyen and B. Choi, "Selection of magnetorheological brake types via optimal design considering maximum torque and constrained volume," *Smart Materials and Structures*, vol. 21, 2012.

[40] J. Nikitczuk, B. Weinberg, and C. Mavroidis, "Control of electrorheological fluid based resistive torque elements for use in active rehabilitation devices," *Smart Materials and Structures*, vol. 16, no. 2, pp. 418–428, Apr. 2007.

[41] J. D. Carlson and T. G. Duclos, "Electrorheological fluid force transmission and conversion device," Jan. 1990, U.S. Classification: 192/21.5 International Classification: : F16D 2700.

[42] E. J. Park, D. Stoikov, L. Falcao da Luz, and A. Suleman, "A performance evaluation of an automotive magnetorheological brake design with a sliding mode controller," *Mechatronics*, vol. 16, no. 7, pp. 405–416, Sep. 2006.

[43] K. H. Gudmundsson, F. Jonsdottir, and F. Thorsteinsson, "A geometrical optimization of a magneto-rheological rotary brake in a prosthetic knee," *Smart Materials and Structures*, vol. 19, no. 3, p. 035023, Mar. 2010.

[44] Q. H. Nguyen and S. B. Choi, "Optimal design of an automotive magnetorheological brake considering geometric dimensions and zero-field friction heat," *Smart Materials and Structures*, vol. 19, no. 11, p. 115024, Nov. 2010.

[45] A. Shafer and M. Kermani, "On the feasibility and suitability of MR fluid clutches in Human-Friendly manipulators," *Mechatronics, IEEE/ASME Transactions on*, vol. 16, no. 6, pp. 1073 –1082, Dec. 2011.

[46] T. Kikuchi, K. Ikeda, K. Otsuki, T. Kakehashi, and J. Furusho, "Compact mr fluid clutch device for human-friendly actuator," *Journal of Physics: Conference Series*, vol. 149, p. 012059, Feb. 2009.

[47] H. Guo and W. Liao, "Optimization of a multifunctional actuator utilizing magnetorheological fluids," in *Advanced Intelligent Mechatronics (AIM), 2011 IEEE/ASME International Conference on*, 2011, pp. 67 –72.

[48] M. Avraam, "Mr-fluid brake design and its application to a portable muscular rehabilitation device," Ph.D. dissertation, Ph. D. thesis, Université Libre de Bruxelle, Bruxelle, Belgium, 2009.

[49] E. J. Park, L. F. a. da Luz, and A. Suleman, "Multidisciplinary design optimization of an automotive magnetorheological brake design," *Computers & Structures*, vol. 86, no. 3–5, pp. 207–216, Feb. 2008.

[50] H. H. Zhang, C. R. Liao, W. M. Chen, and S. L. Huang, "A magnetic design method of MR fluid dampers and FEM analysis on magnetic saturation," *Journal of Intelligent Material Systems and Structures*, vol. 17, no. 8-9, pp. 813–818, Jan. 2006.

[51] L. Yang, F. Duan, and A. Eriksson, "Analysis of the optimal design strategy of a magnetorheological smart structure," *Smart Materials and Structures*, vol. 17, no. 1, p. 015047, Feb. 2008.

[52] N. Guo, H. Du, and W. Li, "Finite element analysis and simulation evaluation of a magnetorheological valve," *The International Journal of Advanced Manufacturing Technology*, vol. 21, pp. 438–445, 2003, 10.1007/s001700300051.

[53] B. Liu, W. H. Li, P. B. Kosasih, and X. Z. Zhang, "Development of an MR-brake-based haptic device," *Smart Materials and Structures*, vol. 15, no. 6, pp. 1960–1966, Dec. 2006.

[54] C. S. Zhu, "The response time of a magnetorheological fluid squeeze film damper rotor system," *Key Engineering Materials*, vol. 334-335, pp. 1085–1088, 2007.

[55] J. Koo, F. D. Goncalves, and M. Ahmadian, "A comprehensive analysis of the response time of MR dampers," *Smart Materials and Structures*, vol. 15, no. 2, pp. 351–358, 2006.

[56] Basf The Chemical Company. http://www.inorganics.basf.com. [Online]. Available: http://www.inorganics.basf.com

[57] Lord Corporation. Avaliable MR fluids:. http://www.lord.com/products-and-solutions/magneto-rheological-

[58] Q. H. Nguyen, J. C. Jeon, and S. B. Choi, "Optimal design of an hybrid magnetorheological brake for Middle-Sized motorcycles," *Applied Mechanics and Materials*, vol. 52-54, pp. 371–377, Mar. 2011.

[59] D. Lampe, A. Thess, and C. Dotzauer, "Mrf-clutch-design considerations and performance," *Transition*, vol. 3, p. 10, 1998.